[6] —, "A new analysis technique for time series data," in *Proc. NATO Advanced Study Inst. Signal Processing, Emphasis Underwater Acoust.*, Enschede, The Netherlands.
[7] J. Durbin, "The fitting of time-series models," *Rev. Intern. Statist*, vol. 28, pp. 233-244, 1960.
[8] N. Levinson, "The Wiener RMS (root mean square) error criterion in filter design and prediction," *J. Math. Phys.*, vol. 25, pp. 261-278, Jan. 1947, also in Appendix B in N. Wiener, *Extrapolation, Interpolation, and Smoothing Stationary Time Series with Engineering Applications*. New York: Technology Press and Wiley, 1949.
[9] A. H. Nuttall, "Spectral analysis of a univariate process with bad data points, via maximum entropy and linear predictive techniques," NUSC Tech. Rep. 5303, Naval Underwater Systems Center, New London, CT, Mar. 26, 1976.

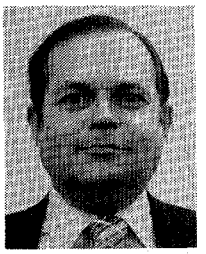

Thomas E. Barnard (M'72) was born in Oklahoma City, OK, on December 5, 1941. He received the Sc.B. degree in applied mathematics from Brown University, Providence, RI, in 1963.

After one year with the General Electric Military Communications Department in Oklahoma City, he spent 14 years with the Services and Equipment Groups of Texas Instruments. Since 1979, he has been with Chesapeake Instrument Division of Gould Inc. His technical interests lie in digital signal processing–time series analysis, array processing, computer roundoff error propagation, target motion analysis, and related topics.

Mr. Barnard is a member of the American Geophysical Union.

High-Speed Coherence Processing Using the Sectionalized Fourier Transform

ALBERT A. GERLACH, SENIOR MEMBER, IEEE

Abstract—**The sectionalized Fourier transform of a band-limited signal (defined as a Fourier transform which is computed over incremented temporal sections of the function) is equivalent to basebanding, filtering, and sampling the signal in the time domain. Spectral windowing is employed, through appropriately summing a sequence of the Fourier transform bins, to control the passband and leakage characteristics of the resulting filter. This in turn controls the distortion of the signal induced as a result of the transform process. The use of the sectionalized Fourier transform is exploited to conveniently and rapidly map the cross-correlation envelope of narrow-band signals over the time-register Doppler-ratio (ambiguity) plane. By using the ambiguity kernel exp ($i2\pi\alpha ft$) as an approximation of signal time compression (or expansion), the coherence between transformed signals (along the Doppler-ratio axis) may further be expedited through use of the discrete Fourier transform. The resulting error is negligible when the time-bandwidth product of the process is less than the inverse of the maximum Doppler ratio employed. The resulting algorithms have proved advantageous in underwater acoustic applications. It is concluded that the sectionalized Fourier Transform has many applications in time-domain signal processing using modern array digital computers.**

INTRODUCTION

WITH the advent of the fast Fourier transform (FFT) algorithm in the mid-1960's [1]-[3] and the corresponding advances in digital computer architecture (in particular, in array processors), giant strides have been made in the rapid computation of complex functions which earlier were considered impractical. More recently, interest has evolved in techniques for estimating the magnitude-squared coherence (MSC) function [4]-[16], and in means for rapidly mapping this estimate over the two-dimensional ambiguity plane [17]-[20]. These techniques invariably involve computing the Fourier transform of the relevant temporal functions in a piecewise or sectionalized manner, and algorithms for computing MSC estimates (using the FFT and modern array processors) have proven highly successful. Unfortunately, knowledge of these techniques (in their entirety) has not been widely disseminated. Nor has the role of the sectionalized Fourier transform in signal processing applications been thoroughly understood by the user community. This report is therefore devoted to developing the fundamental role that the sectionalized Fourier transform plays in temporal signal processing, and to developing a high-speed algorithm for estimating the normalized correlation envelope (NCE) function over the two-dimensional ambiguity surface.

Manuscript received May 29, 1980; revised October 29, 1981. This work was supported by the Tactical Technology Office of the Defense Advanced Research Projects Agency under ARPA Order 3074.

The author is with the Acoustics Division, Naval Research Laboratory, Washington, DC 20375.

SIGNAL TRANSFORMATION

Two approaches will be taken to demonstrate the role of the sectionalized Fourier transform (SFT) in temporal signal processing. In either approach it is shown that the SFT can serve to simply baseband, filter, and sample a narrow-band signal. Due to the filtering action, however, some degree of signal

U.S. Government work not protected by U.S. copyright

distortion is inevitable unless the signal is a constant frequency sinusoid. Reducing the distortion to a tolerable level is achieved through spectral windowing; i.e., to appropriately shape and flatten (or level) the filter response. In the first approach attention is given to the nature and characteristics of the signal distortion function. The tradeoff between the signal and SFT parameters is defined to limit the expected degradation to a tolerable level. In the revisited approach to signal transformation, the basic problem of signal distortion will be evaded by assuming that the spectral power of the signal is bounded within a finite section of the signal spectrum. The two approaches complement one another and yield an insight into the temporal characteristics of the transformation algorithms.

Signal Description and Representation

Over an extended analysis time (approximately T seconds) a narrow-band signal may be represented as

$$u(t) = A(t)e^{i\Psi(t)} \tag{1a}$$

where the phase function $\Psi(t)$ takes the form

$$\Psi(t) = 2\pi\left[f_c t + \int_0^t v(x)\,dx\right] + \phi_0. \tag{1b}$$

The instantaneous frequency (or inverse wave-period) of the signal is defined as

$$\frac{1}{2\pi}\dot{\Psi}(t) = f_c + v(t) \tag{1c}$$

where f_c is the mean frequency and $v(t)$ is the zero-mean frequency fluctuation over the analysis interval. (A "dot" over the variable is used to denote the time derivative.)

In the analyses to follow, two subintervals of time T_1 and T_2 are to be employed such that $T_1 \leqslant T_2$ and T_1 is much less than the extended analysis time.

Letting $f_c T_2 = k_0 + \delta_c$ ($|\delta_c| \leqslant 1/2$) and letting $r = T_2/T_1$, the time series $u(mT_1)$ becomes

$$u(mT_1) = A(mT_1)\,e^{i\Psi(mT_1)} = e^{i2\pi mk_0/r}u_0(mT_1) \tag{2a}$$

where

$$u_0(mT_1) = A(mT_1)\,e^{i[2\pi(m/r)g_0(mT_1)+\phi_0]} \tag{2b}$$

and

$$g_0(t) = \delta_c + \frac{T_2}{t}\int_0^t v(x)\,dx. \tag{2c}$$

The sampled time series $u_0(mT_1)$ represents the baseband of the time series $u(mT_1)$ referenced to the frequency k_0/T_2, and the variable $g_0(mT_1)$ is a running-time average (taken at mT_1) of the instantaneous frequency deviation (relative to baseband) measured in units of $1/T_2$. [The merit of this form of notation will become evident when we consider the sectionalized Fourier transform of the signal $u(t)$.]

Sectionalized Fourier Transform

Over the time interval T_2 centered at mT_1, the sectionalized Fourier transform (SFT) of $u(t)$ is defined as

$$U_m(k_0+n) = \frac{1}{T_2}\int_{mT_1-T_2/2}^{mT_1+T_2/2} u(t)\,e^{-i2\pi(k_0+n)t/T_2}\,dt$$

$$= u_0(mT_1)\,e^{-i2\pi mn/r} \cdot \int_{-T_2/2}^{T_2/2} A_m(t)\,e^{i2\pi[g_m(t)-n]t/T_2}\,dt/T_2 \tag{3a}$$

where

$$A_m(t) = A(mT_1 + t)/A(mT_1) \tag{3b}$$

and

$$g_m(t) = \delta_c + \frac{T_2}{t}\int_0^t v(mT_1 + x)\,dx. \tag{3c}$$

(Care must be exercised in the interpretation and use of (3b). The amplitude function $A_m(t)$ is artificial in the sense that $A(mT_1)$ is inserted in the denominator in order to factor out $u_0(mT_1)$ in (3a). It is possible therefore for $A(mT_1)$ to be zero, in which case $A_m(t)$ makes no sense. However, in this event $u_0(mT_1)$ is zero, and the factor $A_m(t)$ should rightfully equal only the numerator term. For many practical applications, $A(mT_1 + t)$ will be essentially constant over the time interval T_2, avoiding the possibility of singularities.)

The form of (3a) reveals that the SFT of $u(t)$ yields the product of the sampled baseband signal $u_0(mT_1)$ and a distortion factor. The distortion factor is a function of the spectral selectivity of the SFT and the static and dynamic characteristics of the signal. Our object will therefore be to process the SFT to achieve an output transform which approaches $u_0(mT_1)$ over a specified signal center-frequency and bandwidth.

Spectral Windowing

A study of (3) suggests the use of a spectral window comprised of J sequential frequency bins n, approximately centered at the frequency k_0/T_2. Therefore let

$$V_m(k_0; J) = \sum_{n=-n_0}^{J-n_0-1} e^{i2\pi mn/r}U_m(k_0+n)$$

$$= u_0(mT_1)\,D_m(g_m; J) \tag{4a}$$

where

$$D_m(g_m; J) = \int_{-T_2/2}^{T_2/2} A_m(t)\,e^{i2\pi g_m(t)t/T_2} \cdot \sum_{n=-n_0}^{J-n_0-1} e^{i2\pi nt/T_2}\,dt/T_2 \tag{4b}$$

is the resulting distortion function and where J and n_0 are chosen to essentially constrain the signal power within the spectral window. The summation within the above integral may be recognized as the Dirichlet kernel [21], [22]. The sum reduces to [23]

$$1 + 2\sum_{n=1}^{(J-1)/2}\cos(2\pi nt/T_2) = \frac{\sin(\pi Jt/T_2)}{\sin(\pi t/T_2)} \text{ (when } J \text{ is odd)}$$

or

$$2e^{\pm i\pi t/T_2} \sum_{n=1}^{J/2} \cos\left[\pi(2n-1)t/T_2\right]$$

$$= e^{\pm i\pi t/T_2} \frac{\sin(\pi Jt/T_2)}{\sin(\pi t/T_2)} \text{ (when } J \text{ is even).}$$

(The exponential factor, when J is even, results from the spectral window being centered midway between two spectral bins of the SFT. The sign of the exponent depends on whether the center of the window is located one-half bin-width below or above the spectral bin k_0.)

Using the Dirichlet kernel in (4b), the distortion function becomes

$$D_m(g_m; J) = \int_{-T_2/2}^{T_2/2} A_m(t) \frac{\sin(\pi Jt/T_2)}{\sin(\pi t/T_2)} \cdot e^{i2\pi g_m(t)t/T_2}\, dt/T_2 \tag{5}$$

provided that $\pm 1/2$ is added to the parameter δ_c [in (3c)] when J is even. (Assuming that $v(t)$ is symmetrically distributed, the value 1/2 is subtracted when δ_c is positive and added when δ_c is negative. This procedure is required if the spectral window is to most efficiently span the spectral bandwidth of the signal.)

Properties of the Distortion Function

In addition to the window parameter J, the distortion function is dependent on the spectral characteristics of the signal $u(t)$. When the signal dynamic characteristics are sufficiently slowly varying, such that $A(t)$ and $v(t)$ are essentially constant over time intervals of T_2 s, the distortion function is real and equal to the spectral window function $W_J(x_m)$. That is

$$D_m(x_m; J) = W_J(x_m) = \int_0^1 \frac{\sin(\pi Jt/2)}{\sin(\pi t/2)} \cos(\pi x_m t)\, dt \tag{6a}$$

where $x_m = \delta_c + T_2 v(mT_1)$ when J is odd or $\delta_c \mp 0.5 + T_2 v(mT_1)$ when J is even. By expressing the Dirichlet kernel by its equivalent trigonometric series and carrying out the integration prior to summing, $W_J(x)$ may be shown to be

$$W_J(x) = \sum_{n=-(J-1)/2}^{(J-1)/2} \frac{\sin\pi(x-n)}{\pi(x-n)}$$

$$= \frac{\sin\pi x}{\pi x}\left[1 + 2\sum_{n=1}^{(J-1)/2} (-1)^n \frac{x^2}{x^2-n^2}\right] \tag{6b}$$

when J is odd, or

$$W_J(x) = \sum_{n=\mp(J/2)}^{\pm[(J/2)-1]} \frac{\sin\pi(x-n)}{\pi(x-n)}$$

$$= \frac{2}{\pi}\cos\pi(x \pm 0.5) \sum_{n=1}^{J/2} (-1)^n \frac{n-0.5}{(x \pm 0.5)^2 - (n-0.5)^2} \tag{6c}$$

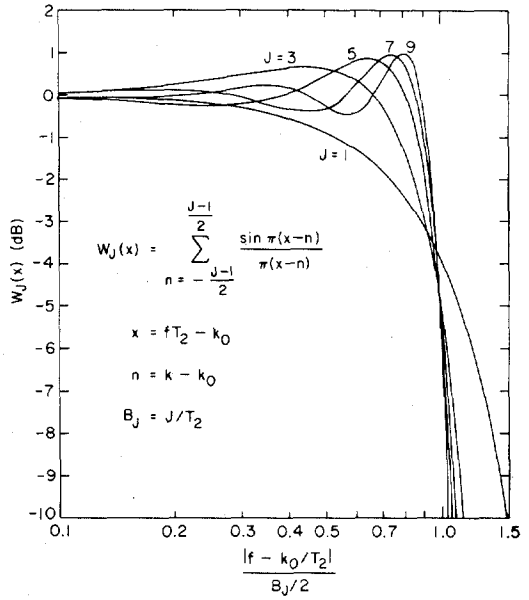

Fig. 1. Passband characteristics of the spectral window function $W_j(x)$ for J odd.

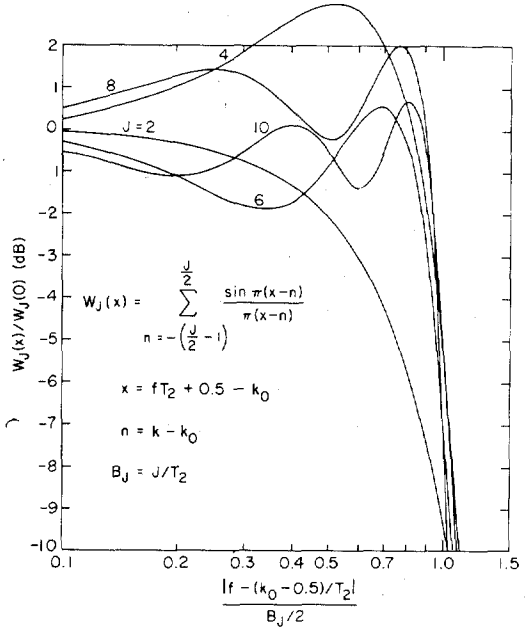

Fig. 2. Passband characteristics of the spectral window function $w_j(x)$ for J even.

when J is even. (The shift of 1/2 in the latter relation is due to the fact that the center of the spectral window is $\pm$ one-half bin-width from the k_0th bin.) A plot of $W_J(x)$ as a function of the normalized frequency is displayed in Figs. 1 and 2 for selected odd and even values of J, respectively. The filter characteristics are somewhat smoother over the filter passband J/T_2 when J is odd. However, as J gets larger, the difference in the odd versus even passband characteristics becomes proportionately smaller.

In addition to the static window characteristics, the signal distortion is also a function of the signal dynamics. The expected value of the distortion function may be shown to ap-

TABLE I
MAGNITUDE AND PHASE OF $D_m(g_m; J)$ AS A FUNCTION OF $\Delta x_m/J$ FOR THE INDICATED VALUES OF J ($x_m = 0$)

$\frac{\Delta x_m}{J}$	$D_m(g_m; J)$	$J = 1$	3	5	7	9
0	Magnitude	1.000	1.000	1.000	1.000	1.000
	Phase (Deg.)	0.00	0.00	0.00	0.00	0.00
± 0.2	Magnitude	0.999	1.013	0.985	1.016	0.986
	Phase (Deg.)	±3.00	∓1.81	±1.04	∓0.50	±0.16
± 0.4	Magnitude	0.996	1.051	0.949	1.035	0.988
	Phase (Deg.)	±5.99	∓2.91	±0.49	±1.04	∓1.67
± 0.6	Magnitude	0.990	1.105	0.924	1.009	1.044
	Phase (Deg.)	±8.98	∓2.85	∓2.56	±3.90	∓2.00
± 0.8	Magnitude	0.983	1.165	0.945	0.924	1.085
	Phase (Deg.)	±11.96	∓1.53	∓7.17	±4.85	±2.42
± 1.0	Magnitude	0.973	1.224	1.026	0.832	1.010
	Phase (Deg.)	±14.92	±0.94	∓10.71	∓0.25	±8.61

proach one when J is large and the spectral bandwidth of the signal is essentially bound within the filter passband (see Appendix). Since the expected value of the distortion function was computed using ensemble averages, it will prove informative to compute this function over the time interval T_2 for a representative case. Consider then that over the relevant T_2 time interval, the amplitude factor $A_m(t)$ is constant and the frequency fluctuation $v(t)$ can be represented by the truncated Taylor series

$$v(mT_1 + x) = v(mT_1) + \dot{v}(mT_1)x. \tag{7a}$$

From (3c) and the definition of x_m [following (6a)]

$$g_m(t) = x_m + 0.5\Delta x_m t/T_2 \tag{7b}$$

where

$$\Delta x_m = \dot{v}(mT_1)T_2^2. \tag{7c}$$

(In the normalized units of $1/T_2$ Hz, the discrete variable x_m is a measure of the instantaneous frequency deviation from the window center-frequency, and Δx_m is a measure of the change in instantaneous frequency over the SFT interval T_2.) From (5) then, the distortion function becomes

$$D_m(g_m; J) = \int_0^1 e^{i(\pi/4)\Delta x_m t^2} \frac{\sin(\pi Jt/2)}{\sin(\pi t/2)} \cos(\pi x_m t)\, dt. \tag{8}$$

Except when Δx_m is zero (in which case the distortion function reduces to the spectral window function), the distortion will be a complex number, resulting in both amplitude and phase distortion. To provide an indication of the degree of distortion that can exist, (8) has been computed as a function of Δx_m (with $x_m = 0$) for various values of the parameter J. The results are tabulated in Table I. (The ratio $\Delta x_m/J$ is the fraction of the spectral window over which the instantaneous frequency varies in the time interval T_2. Thus when x_m is zero, the frequency will be constrained within the spectral window for $\Delta x_m/J$ less than one.) The data in Table I indicate that the distortion will be relatively minor under the stipulated conditions. The distortion has been computed for values of x_m other than zero and found to be no more serious than that shown in the table, as long as the instantaneous frequency is constrained to fall within the bounds of the spectral window. In the particular case where $J = 1$ and $x_m = 0$, the distortion reduces to

$$D_m(g_m; 1) = \frac{C(\sqrt{|\Delta x_m|/2}) + iS(\sqrt{|\Delta x_m|/2})}{\sqrt{|\Delta x_m|/2}} \tag{9}$$

where $S(\cdots)$ and $C(\cdots)$ are the Fresnel sine and cosine integrals of the indicated argument [24].

SIGNAL TRANSFORMATION REVISITED

Fourier Series Representation

To obtain a deeper insight into the sectionalized Fourier transform method of signal filtering, basebanding, and sampling, a second approach will be taken which is more macroscopic in content. Utilizing the results of sampling theory [25], [26], it has been shown that over the time span of $mT_1 - T_2/2 \leqslant t \leqslant mT_1 + T_2/2$, the function $u(t)$ may be expressed by the Fourier series

$$u(t) = \sum_{k=0}^{\infty} U_m(k) e^{i2\pi kt/T_2} \tag{10}$$

where $U_m(k)$ is the sectionalized Fourier transform of $u(t)$ [(3)] taken over the indicated time interval. Although the value of $U_m(k)$ will (in general) be nonzero over all k, it is common practice to set bounds on the range of k over which $|U_m(k)|$ is significant for certain classes of signals.[1] If then $u(t)$ is a band-limited signal whose significant spectral energy can be said to be bounded within a contiguous sequence of J spectral bins centered at approximately $k = k_0$, a suitable approximation of $u(t)$ over the indicated temporal span would be

$$\tilde{u}(t) = \sum_{k=k_0-n_0}^{k_0+J-n_0-1} U_m(k) e^{i2\pi kt/T_2}$$

$$= e^{i2\pi k_0 t/T_2} \sum_{n=-n_0}^{J-n_0-1} U_m(k_0 + n)\, e^{i2\pi nt/T_2} \tag{11a}$$

or

$$\tilde{u}_0(t) = e^{-i2\pi k_0 t/T_2} \tilde{u}(t)$$

$$= \sum_{n=-n_0}^{J-n_0-1} U_m(k_0 + n) e^{i2\pi nt/T_2}. \tag{11b}$$

Consequently, from (4a) and (11b)

$$\tilde{u}_0(mT_1) = V_m(k_0; J) = u_0(mT_1) D_m(g_m; J). \tag{12}$$

The above relation demonstrates that the sectionalized Fourier transform can serve to baseband, filter, and sample a band-limited function without basically changing the temporal

[1] Although a signal cannot be both band- and time-limited in a pure theoretical sense, this concept has proven quite useful in practical applications. An excellent discussion of the problem is found in [21, pp. 121–132].

characteristics of the function. In addition, the relative simplicity of the FFT algorithm permits these processing operations to be performed with ease on modern digital computers. The factor $D_m(g_m; J)$, given in (5), provides a measure of the distortion induced by the process, so that some basis is available for the selection of the parameters T_2 and J. The criterion for the selection of the sampling rate $1/T_1$ is also well defined. To avoid undersampling, the sampling rate should be equal to or greater than the (two-sided) filter bandwidth $B_J = J/T_2$, or T_1 should be equal to or less than the Nyquist interval T_2/J [27].

Equivalent Temporal Window

The temporal counterpart of spectral filtering (or windowing) in harmonic analysis is to shade or to weight the function $u(t)$ over the time window $mT_1 - T_2/2 \leqslant t \leqslant mT_1 + T_2/2$ [28], [29]. The temporal window function, equivalent to the spectral window $W_J(x)$, is simply the inverse Fourier transform of $W_J(fT_2)$. Therefore, from (6b) and (6c)

$$w_J(t) = T_2 \int_{-\infty}^{\infty} W_J(fT_2) e^{i2\pi ft}\, df$$

$$= 1 + 2 \sum_{n=1}^{(J-1)/2} \cos(2\pi nt/T_2)$$

$$= \frac{\sin(\pi Jt/T_2)}{\sin(\pi t/T_2)} \qquad (|t| \leqslant T_2/2) \tag{13a}$$

for J odd, and

$$w_J(t) = e^{\pm i\pi t/T_2}\, 2 \sum_{n=1}^{J/2} \cos[\pi(2n-1)t/T_2]$$

$$= e^{\pm i\pi t/T_2} \frac{\sin(\pi Jt/T_2)}{\sin(\pi t/T_2)} \qquad (|t| \leqslant T_2/2). \tag{13b}$$

for J even. (The complex exponential factor for J even is a consequence of the spectral window being centered midway between two spectral bins.) A plot of the temporal window function for various values of J is shown in Fig. 3. For $J = 1$, the weighting is constant. For $J = 2$, the weighting magnitude is a simple cosine function. As J becomes larger, the temporal window (Dirichlet kernel) more closely approaches a $(\sin x)/x$ function over the interval T_2.

If now, over the time interval $mT_1 - T_2/2 \leqslant t \leqslant mT_1 + T_2/2$, one defines a new function $v(t)$, where

$$v(t) = w_J(t - mT_1)\, u(t), \tag{14}$$

its sectionalized Fourier transform can readily be shown to be

$$\frac{1}{T_2} \int_{mT_1 - T_2/2}^{mT_1 + T_2/2} w_J(t - mT_1)\, u(t) e^{-i2\pi kt/T_2}\, dt$$

$$= \sum_{n=-n_0}^{J-n_0-1} e^{i2\pi mn/r} U_m(k+n) = V_m(k; J) \tag{15a}$$

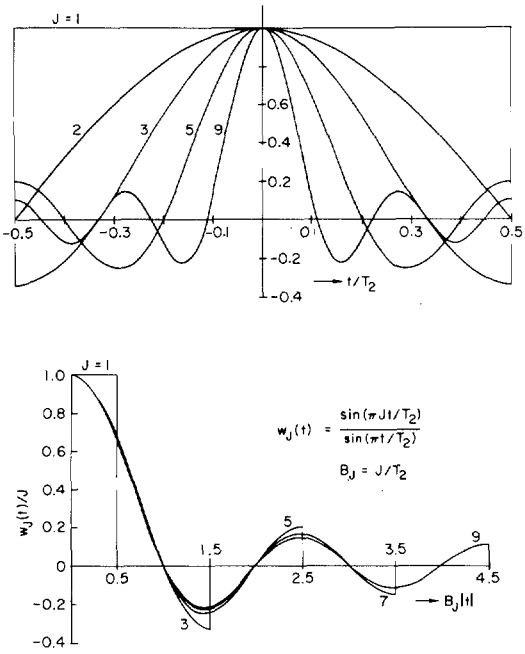

Fig. 3. Temporal window function $w_J(t)$ for selected values of J.

where

$$U_m(k) = \frac{1}{T_2} \int_{mT_1 - T_2/2}^{mT_1 + T_2/2} u(t) e^{-i2\pi kt/T_2}\, dt \tag{15b}$$

and where n_0 is $(J-1)/2$ when J is odd, and $J/2$ or $J/2 - 1$ when J is even [depending on the sign of the exponent in (13b)]. Equation (15a) is identical to (4a), except that here the spectral bin k is general and need not be restricted to fitting any particular center frequency. Thus the spectral window may be incremented across the frequency band in steps of one to J bin-widths. Computationally, it is more economical to implement the window function in the spectral domain when only one or a few spectral bands need be examined for signals. There is also merit in the fact that k may be indexed in less than J increments to smooth or effectively eliminate any "picket-fence" or "scallop" effect between windows [28].

A study of the temporal window function (Fig. 3) reveals that the significance of $u(t)$, in the formation of its Fourier transform, decreases rapidly as t deviates from $\pm T_2/2J$. That is, as $|t|$ becomes greater than $1/2B_J$, the weight given to $u(t)$ becomes appreciably reduced, so that its significance in the construction of the resulting Fourier transform $U_m(k)$ is reduced. This is why the value of Δx_m, in the distortion function $D_m(g_m; J)$, can become proportionally larger with J without seriously altering the transform characteristics (see Table I). The restrictions on the rate of change in the amplitude function $A(t)$ is also proportionally reduced. Another way of looking at it is that as J becomes larger, the bandwidth of the spectral window increases (assuming T_2 remains fixed). And consequently the signal dynamics can be correspondingly more rapid (spreading the power spectral density of the signal)

to fill the wider window, without seriously degrading the transformed output.

Doppler-Induced Distortion

When a signal source is in motion in a transmission medium, the spectral energy of the signal suffers a Doppler shift. The effect of the Doppler shift is to compress (or expand) the time scale of the original signal [30]. Thus, the signal $u(t)$ is transformed into $u\{(1+\alpha_0)t\}$ where α_0 ($\alpha_0 \ll 1$) is known as the time scale-factor shift or Doppler ratio. From (1) and (2) it is easy to show that

$$u_0\{(1+\alpha_0)mT_1\} = A_{2,m}u_0(mT_1)e^{i2\pi m\alpha_0[f_c+v_2(mT_1)]T_1} \tag{16a}$$

where $u_0\{(1+\alpha_0)mT_1\}$ and $u_0(mT_1)$ are the respective band-shifted signals (relative to k_0/T_2 Hz), and where

$$A_{2,m} = A\{(1+\alpha_0)mT_1\}/A(mT_1) \tag{16b}$$

and

$$v_2(mT_1) \approx v\{(1+\alpha_0/2)mT_1\}. \tag{16c}$$

When α_0 is sufficiently small so that $m\alpha_0 \leqslant r/J$, $A_{2,m}$ will be close to unity. (The amplitude distortion factor $A_{2,m}$ is due to the time compression of the Doppler-shifted signal.) For the purposes of this paper, $A(t)$ is considered to vary sufficiently slowly so that insignificant error will result in assuming that $A_{2,m} = 1$.

Since the effect of the time compression is to slightly shift the spectral power of the signal $u(t)$ into a new band, it may be desirable to translate the Fourier transform sequence (spectral window) to accommodate this Doppler shift. To optimumly accomplish this, let

$$\alpha_0 f_c T_2 = n_\alpha + \epsilon, \quad (\text{where } -1/2 \leqslant \epsilon \leqslant 1/2). \tag{17a}$$

Following the procedure given in (11), it may be verified that

$$\begin{aligned} e^{-i2\pi mn_\alpha/r}&\tilde{u}_0\{(1+\alpha_0)mT_1\} \\ &= V_{2,m}(k_0+n_\alpha; J) \\ &= \sum_{n=-n_0}^{J-n_0-1} e^{i2\pi mn/r}U_{2,m}(k_0+n_\alpha+n) \\ &\approx \tilde{u}_0(mT_1)e^{i2\pi m[\epsilon/r+\alpha_0 T_1 v_2(mT_1)]} \end{aligned} \tag{17b}$$

where $U_{2,m}(k)$ is the sectionalized Fourier transform of $u\{(1+\alpha_0)t\}$. The translation of the Fourier transform sequence by n_α has the effect of centering the spectral window on the Doppler-translated signal spectrum to minimize the output signal distortion. (If the spectral window is sufficiently broad to adequately encompass the Doppler shift, this step would be unnecessary.) Another way of looking at it is that the far left-hand side of (17b) is the baseband for the Doppler-shifted signal. Although a frequency translation of k_0/T_2 represents baseband for the signal $u(t)$, a frequency translation of $(k_0+n_\alpha)/T_2$ is required to represent baseband for the Doppler-shifted signal $u\{(1+\alpha_0)t\}$.

For our purposes we shall assume that the bandwidth of the spectral window is sufficient to ignore the Fourier transform distortion factor (permitting us to drop the "tilde" from the functional relations). And we shall assume that $m\alpha_0$ is sufficiently small to ignore the amplitude distortion factor $A_{2,m}$. (We shall later develop the restrictions on α_0 and the analysis time to permit this realization.) The significant relations relative to Doppler-shifted signals are then

$$\begin{aligned} u_0\{(1+\alpha_0)mT_1\} &= V_{2,m}(k_0; J) \\ &= e^{i2\pi mn_\alpha/r}V_{2,m}(k_0+n_\alpha; J) \\ &= e^{i2\pi m\alpha_0 f_c T_1}V_m(k_0; J)e^{i2\pi m\alpha_0 T_1 v_2(mT_1)}. \end{aligned} \tag{18}$$

The first exponential factor in the right-hand side of (18) reveals that a Doppler shift produces a linearly varying phase rotation on the original signal. The rate of phase rotation is proportional to the product of α_0 and the mean signal frequency f_c. (For a CW signal this will be the only phase distortion.) However, the zero-mean fluctuating frequency $v(t)$ introduces a nonlinear phase-shift which must also be taken into consideration. The degradation effect of this latter factor will be addressed in a latter section of the paper.

Effect of Time Shifts

Consider now the effect of a simple time translation τ_0 on the signal $u(t)$. Letting $\tau_0 = (m_0+\epsilon_1)T_1$ where $-1/2 \leqslant \epsilon_1 < 1/2$, it is easy to show that

$$\begin{aligned} &u_0(mT_1+\tau_0) \\ &\quad = A_{1,m}u_0\{(m+m_0)T_1\}\, e^{i2\pi\epsilon_1[f_c+v_1\{(m+m_0)T_1\}]T_1} \end{aligned} \tag{19a}$$

where $u_0(mT_1+\tau_0)$ and $u_0\{(m+m_0)T_1\}$ are the respective basebanded signals, and where

$$A_{1,m} = A(mT_1+\tau_0)/A\{(m+m_0)T_1\} \simeq 1 \tag{19b}$$

and

$$v_1(mT_1) = v\{(m+\epsilon_1/2)T_1\}. \tag{19c}$$

(Since the amplitude functions in (19b) differ in time by less than $1/2T_1$, negligible error will result in assuming that $A_{1,m} = 1$.)

Again, following the procedure given in (11), it may be verified that

$$\begin{aligned} \tilde{u}_0(mT_1+\tau_0) &= V_{1,m}(k_0; J) \\ &= \sum_{n=-n_0}^{J-n_0-1} e^{i2\pi mn/r}U_{1,m}(k_0+n) \\ &= e^{i2\pi\epsilon_1[f_c+v_1\{(m+m_0)T_1\}]T_1}V_{m+m_0}(k_0; J) \end{aligned} \tag{20}$$

where $U_{1,m}(k)$ is the sectionalized Fourier transform of $u(t+\tau_0)$.

Assuming that the bandwidth of the spectral window is sufficient to ignore the Fourier transform distortion factor [(12)], the "tilde" may be dropped from the above relation. Consequently, the effect of the residual parameter ϵ_1 is to cause a

TABLE II
INTEGRAL OF THE SQUARE OF THE SPECTRAL WINDOW FUNCTION $W_J(Jx/2)$ OVER THE LIMITS 0 to y [SEE (23)]

y \ J	1	2	3	4	5	6	7	8	9	10
0.10	0.0997	0.1611	0.1005	0.0737	0.0994	0.1186	0.1006	0.0885	0.0995	0.1082
0.15	0.1491	0.2398	0.1517	0.1135	0.1482	0.1727	0.1516	0.1385	0.1486	0.1559
0.20	0.1978	0.3163	0.2040	0.1567	0.1962	0.2219	0.2031	0.1933	0.1979	0.2002
0.25	0.2458	0.3900	0.2575	0.2043	0.2436	0.2664	0.2543	0.2513	0.2480	0.2444
0.30	0.2927	0.4602	0.3123	0.2569	0.2909	0.3075	0.3046	0.3095	0.2994	0.2919
0.35	0.3385	0.5266	0.3684	0.3146	0.3387	0.3468	0.3533	0.3646	0.3518	0.3446
0.40	0.3830	0.5886	0.4255	0.3774	0.3877	0.3866	0.4003	0.4146	0.4042	0.4014
0.45	0.4260	0.6459	0.4832	0.4443	0.4389	0.4290	0.4461	0.4593	0.4551	0.4585
0.50	0.4674	0.6984	0.5409	0.5140	0.4927	0.4761	0.4918	0.5005	0.5034	0.5115
0.55	0.5070	0.7459	0.5978	0.5848	0.5494	0.5294	0.5390	0.5411	0.5492	0.5584
0.60	0.5448	0.7884	0.6531	0.6546	0.6086	0.5892	0.5893	0.5849	0.5941	0.6004
0.65	0.5807	0.8259	0.7059	0.7210	0.6694	0.6546	0.6440	0.6350	0.6406	0.6419
0.70	0.6145	0.8586	0.7552	0.7821	0.7300	0.7229	0.7030	0.6931	0.6916	0.6879
0.75	0.6463	0.8867	0.8003	0.8361	0.7881	0.7901	0.7649	0.7581	0.7487	0.7428
0.80	0.6760	0.9106	0.8403	0.8818	0.8414	0.8516	0.8261	0.8254	0.8107	0.8065
0.85	0.7036	0.9305	0.8749	0.9187	0.8874	0.9034	0.8820	0.8874	0.8723	0.8729
0.90	0.7291	0.9467	0.9038	0.9470	0.9245	0.9430	0.9278	0.9373	0.9257	0.9307
0.95	0.7524	0.9598	0.9269	0.9673	0.9520	0.9700	0.9605	0.9708	0.9640	0.9707
1.00	0.7737	0.9701	0.9447	0.9808	0.9703	0.9859	0.9801	0.9888	0.9851	0.9908
$1+1/J$	0.9028	0.9949	0.9762	0.9959	0.9876	0.9967	0.9919	0.9972	0.9941	0.9976

fixed phase-shift ($2\pi\epsilon_1 f_c T_1$) and a fluctuating phase-shift [due to the fluctuating frequency $v(t)$] on a signal that would be delayed an even multiple of T_1 seconds.

DESIGN CONSIDERATIONS

Noise Power Output

Since the signal channel will generally be contaminated by broad-band noise, it will be of interest to determine the noise output of the filter $W(fT_2)$ inherent in the sectionalized Fourier transform. Assuming a broad-band noise power spectral density of N_0 watts per Hz, the accumulated noise power over the spectral window is (employing Parseval's theorem; see [25, p. 65])

$$P_N = N_0 \int_{-\infty}^{\infty} W_J^2(fT_2)\,df = \frac{2N_0}{T_2}\int_0^{\infty} W_J^2(x)\,dx$$

$$= \frac{2N_0}{T_2^2}\int_0^{T_2/2} |w(t)|^2\,dt = \frac{2N_0}{T_2}\int_0^{1/2} \frac{\sin^2(\pi Jt)}{\sin^2(\pi t)}\,dt$$

$$= N_0 J/T_2 = N_0 B_J \tag{21}$$

where $B_J = J/T_2$ is the bandwidth of the spectral window (see Figs. 1 and 2). (It is also the equivalent noise bandwidth of the window [28].)

Output Signal-to-Noise Ratio

If $p_u(f)$ is the signal power spectral density function and f is frequency, measured relative to the center of the spectral window, the output signal power will be

$$P_u = \int_{-\infty}^{\infty} p_u(f)\,W_J^2(fT_2)\,df. \tag{22}$$

When the signal power is uniformly distributed over the band f_1 to f_2, the output signal power becomes

$$P_u = \langle u^2(t)\rangle \frac{Z_J(y_2) - Z_J(y_1)}{y_2 - y_1} \tag{23a}$$

where $y = 2f/B_J$ and where

$$Z_J(y) = \int_0^y W_J^2(Jx/2)\,dx. \tag{23b}$$

The function $Z_J(y)$ is tabulated in Table II for values of y lying within the main lobe of the spectral window. From (21) and (23) then, the output signal-to-noise power ratio becomes

$$P_u/P_N = \frac{\langle u^2(t)\rangle}{N_0 B_J}\,\frac{Z_J(y_2) - Z_J(y_1)}{y_2 - y_1}. \tag{24a}$$

And, if the signal power spectral density is symmetrically located within the filter window, the relation reduces to

$$P_u/P_N = \frac{\langle u^2(t)\rangle}{N_0 B_J}\,\frac{Z_J(y)}{y}. \tag{24b}$$

For a properly designed system, B_J should be chosen to efficiently contain the signal power without significant excess or spillover. Ideally, y should be one to avoid an excess of unwanted noise and interference. From Table II (and $y = 1$), it is seen that for J greater than one the output signal-to-noise ratio is very nearly ideal. Even for J equal to one, the loss in signal-to-noise ratio is only slightly in excess of one decibel. Consequently, from the standpoint of signal-to-noise ratio, there is no strong motivation for choosing a value of J greater than one.

Spectral Leakage

An important facet in the design of the spectral window (selection of the parameter J) is the spectral leakage resulting from the window sidelobes [28]. These sidelobes will cause signals remote from the window bandwidth to appear at the filter output, even though they are attenuated. And if the re-

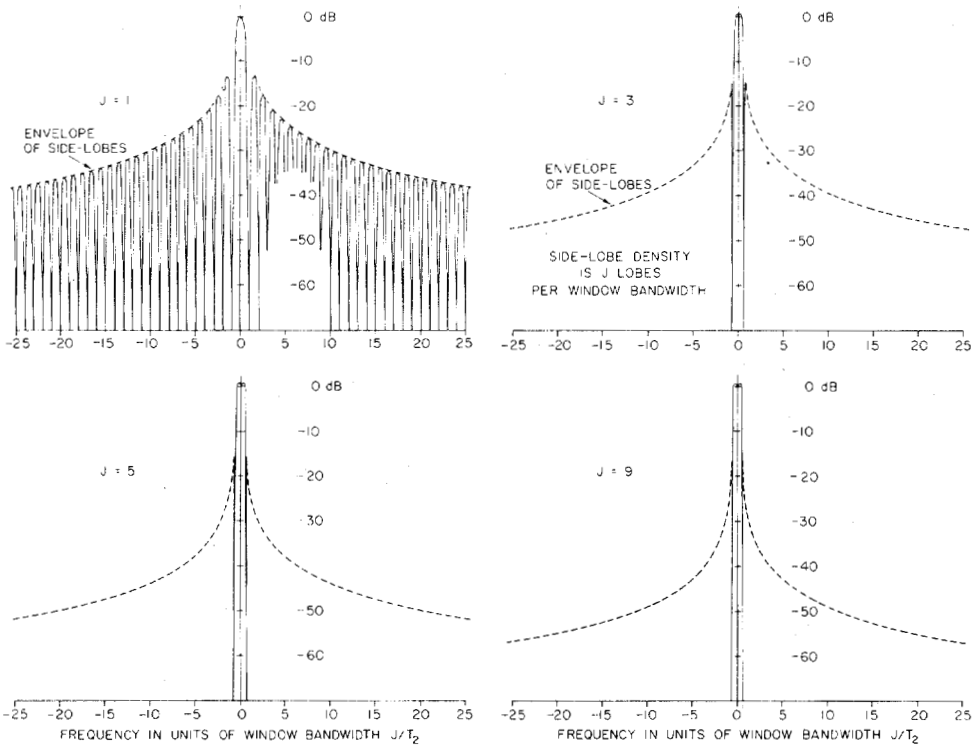

Fig. 4. Sidelobe leakage characteristics of the spectral window function $W_J(x)$ for odd values of the parameter J.

mote signals are sufficiently strong, they can seriously interfere with those signals falling within the filter window. Consequently, it is important that the filter window reject those signals whose spectral energy falls outside of the spectral window to the degree that is practical.

From (6), the magnitude of the spectral window sidelobes is closely approximated by

$$\left|W_J\left(\frac{J}{2}+m\right)\right| = \frac{2}{\pi(J+2m)} \cdot \left|1+2\sum_{n=1}^{(J-1)/2}(-1)^n \frac{(J+2m)^2}{(J+2m)^2-(2n)^2}\right| \tag{25a}$$

when J is odd, or

$$\left|W_J\left(\frac{J+1}{2}+m\right)\right| = \frac{4}{\pi}\left|\sum_{n=1}^{J/2}(-1)^n \frac{2n-1}{(J+2m)^2-(2n-1)^2}\right| \tag{25b}$$

when J is even, where $m = 1, 2, \cdots$ is the sidelobe index along the frequency axis.

For large values of m $(J \ll m)$

$$\left|W_J\left(\frac{J}{2}+m\right)\right| \approx \frac{2}{\pi(J+2m)} = \frac{B_J}{\pi Jf} \quad \text{(for } J \text{ odd)} \tag{26a}$$

and

$$\left|W_J\left(\frac{J+1}{2}+m\right)\right| \approx \frac{2J}{\pi(J+2m)^2} = \frac{B_J^2}{2\pi Jf^2} \quad \text{(for } J \text{ even)} \tag{26b}$$

where f is frequency measured relative to the center of the spectral window. For B_J constant, it is seen that the magnitude of the remote filter sidelobes is inversely proportional to J. A more interesting fact is that the magnitude of the sidelobes decays at a rate of 12 dB/octave of frequency when J is even, and only 6 dB/octave of frequency when J is odd. Thus, from the standpoint of interference rejection it will be more productive to make J even.

Plots of the spectral window characteristics for J odd and even are shown in Figs. 4 and 5. The frequency axis of the curves is scaled in units of the window bandwidth in each case for comparison purposes. The advantage of making J even in lieu of odd is quite apparent. Further, since the sidelobe density is J lobes per window bandwidth, interferring signals whose spectral power is spread over one or more sidelobes will be attenuated approximately 4 dB below the indicated sidelobe envelope.

Correlation Processing

Magnitude-Squared Coherence

The magnitude-squared coherence function (MSC) of two signals $s_1(t)$ and $s_2(t)$ is defined as

$$\Gamma^2(f) = \frac{|S_{12}(f)|^2}{S_{11}(f)S_{22}(f)} \tag{27}$$

where $S_{11}(f)$ and $S_{22}(f)$ are the power spectral densities of $s_1(t)$ and $s_2(t)$, respectively, and $S_{12}(f)$ is the cross-power spectral density (Fourier transform of the cross-correlation function). Note that the MSC will range between zero and one depending upon the magnitude of the cross-power spectral density.

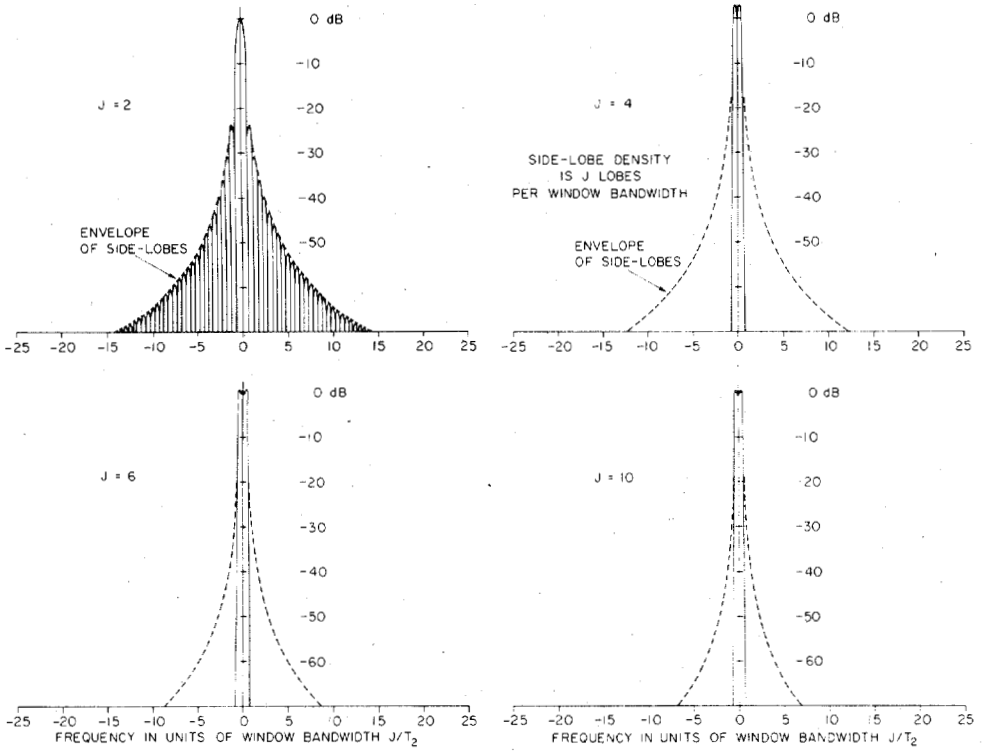

Fig. 5. Sidelobe leakage characteristics of the spectral window function $W_J(x)$ for even values of the parameter J.

Perhaps the most unique property of the MSC is its invariance under linear operations. That is, if $v_1(t)$ and $v_2(t)$ are the result of linear time-invariant operations on $s_1(t)$ and $s_2(t)$, then the MSC of $v_1(t)$ and $v_2(t)$ will be identical to the MSC of $s_1(t)$ and $s_2(t)$ [4]. This will be true even though the correlation coefficient between $v_1(t)$ and $v_2(t)$ may differ radically from the correlation coefficient between $s_1(t)$ and $s_2(t)$. Thus, the square root of the MSC and the correlation coefficient, although somewhat related, are truly different concepts.

MSC Estimate

The magnitude-squared coherence estimate has been defined as [4]

$$\hat{\Gamma}^2(k) = \frac{|\langle S_{1,m}(k) S^*_{2,m}(k)\rangle|^2}{\langle |S_{1,m}(k)|^2\rangle \langle |S_{2,m}(k)|^2\rangle} \tag{28}$$

where the indicated average is computed over a given analysis interval, and $S_m(k)$ is the sectionalized Fourier transform of the relevant temporal function computed over time T_2. (The asterisk denotes the complex conjugate.) In the notation above, the time index is m $(t = mT_1 \leqslant mT_2)$ and the frequency index is k $(f_k = k/T_2)$. The numerator in the above equation forms the estimate of the cross-power spectral density between the two relevant signals $s_1(t)$ and $s_2(t)$.

The MSC estimate has received considerable attention in the literature as a sample test statistic for coherence estimates [4]-[16]. However, depending upon the length of the analysis interval and several other factors, the estimate may not be a good estimate of the MSC. One can readily perceive that the estimate is no longer invariant with linear operations on the two signals, but can vary appreciably depending on the nature of these operations. In fact (as shall be subsequently shown), when the spectral power of the two temporal signals is essentially bounded within the spectral bin-width of the Fourier transform, the square root of the MSC estimate closely approximates the normalized envelope correlation function of the two signals.

Normalized Correlation Envelope

Consider now that $s_1(t)$ and $s_2(t)$ are two real narrowband signals present at two sensors. The normalized two-dimensional correlation function (NC) of the signals (over an extended analysis interval) is defined as [31]

$$\gamma(\tau, \alpha) = \frac{\langle s_1(t-\tau)\, s_2(t+\alpha t)\rangle}{\sqrt{\langle s_1^2(t-\tau)\rangle \langle s_2^2(t+\alpha t)\rangle}} \tag{29}$$

where the indicated averaging is carried out over the analysis interval. The resulting NC can generally be written as the product of a slowly varying correlation envelope (NCE) function $\chi(\tau, \alpha)$, and a sinusoidal carrier function $C(\tau, \alpha)$ [31]. By repeating the NC with τ shifted by one-quarter of a cycle of the carrier frequency, the resulting NC will be in quadrature with the original NC. (The minute shift in τ will not significantly change the value of the correlation envelope function.) Thus, the NCE may readily be computed as the square root of the sum of the squares of the NC and the quadrature NC.

The indicated procedure for determining the NCE is computationally awkward and inefficient. Further, since the desired signals are generally contaminated by noise and interfering signals, some form of filtering is desired around the relevant signals to improve their signal-to-background ratio

prior to correlation. The technique of basebanding and low-pass filtering the relevant signals prior to correlation is a suitable alternative, but this is computationally unattractive if carried out in the normal step-wise fashion. However, the earlier analyses have shown that basebanding and spectral filtering may be accomplished quite readily through the use of the sectionalized Fourier transform. This suggests that the following algorithm may serve as a convenient estimate of the NCE.

$$\hat{\chi}_k(\tau, \alpha) = \frac{|\langle e^{im(q/M)\pi} V_{1,m-m_\tau}(k; J) V^*_{2,m}(k; J)\rangle|}{\sqrt{\langle |V_{1,m-m_\tau}(k; J)|^2\rangle \langle |V_{2,m}(k; J)|^2\rangle}} \tag{30a}$$

where the symbology

$$\langle(\cdots)\rangle \text{ implies } \frac{1}{M} \sum_{m=-M/2}^{M/2-1} (\cdots) \tag{30b}$$

and where m_τ (an integer) reflects the time displacement (tau variable), and q (an integer) reflects the time scale-factor shift or Doppler ratio (alpha variable) between the two signals. The transforms in the relation are defined by (15), with subscripts added to denote the signals within the two k-bin channels being processed. The exponential factor in the numerator of the above relation serves as the ambiguity kernel $\exp(i2\pi\alpha ft)$ [32] to Doppler-shift the transform $V^*_{2,m}(k; J)$. This is suggested from (18) as a method of (approximately) compensating for any time scale-factor shift between the signals in the two channels.[2]

The optimum choice for T_1 in the NCE estimate is the Nyquist interval $T_2/J = 1/B_J$ ($r = T_2/T_1 = J$). With this choice, the total analysis time is MT_1 and the correlation integration time is

$$T = (M - 1)T_1 = (M - 1)/B_J \tag{31a}$$

or

$$M = B_J T + 1. \tag{31b}$$

An explicit expression for the τ variable is, of course,

$$\tau = m_\tau T_1 = m_\tau / B_J. \tag{32}$$

However, the explicit Doppler ratio for a given signal will depend on the mean frequency of that signal over the processor analysis interval [(16a)]. A suitable estimate of the Doppler ratio is given by

$$\hat{\alpha} = \frac{qJ}{2Mk} < \frac{q}{2f_k T} \tag{33a}$$

where $f_k = k/T_2$ is the approximate center-frequency of the spectral window. When k is optimum for a given signal (viz., when the spectral window is most nearly centered about the signal spectrum), the error in the estimate will be

$$\left|\frac{\hat{\alpha} - \alpha}{\alpha}\right| = \frac{|\delta_c|}{k} \leqslant \frac{B_J}{2Jf_k} \tag{33b}$$

where δ_c ($|\delta_c| \leqslant 1/2$) is the difference between f_c and the nearest harmonic k/T_2. The choice of the index q to vary the Doppler ratio in increments of approximately $1/2f_cT$ was made to limit the "picket-fence" or "scallop" loss in the α-dimension to less than 1 dB [28].

Computation of NCE Estimate

Computing the two-dimensional NCE estimate must certainly be considered a formidable task as a result of the variables m_τ and q over which a correlation surface is mapped. In practice, the number of points required to satisfactorily map the surface can range from several thousand to the tens of thousands. However, the present state-of-the-art in computer technology (using modern array processors) is such that adequate computational speed is available, providing the processing algorithms are suitably matched to the computer architecture. In the case of the transforms $V_m(k; J)$, these are ideally suited for array processing using conventional DFT (discrete Fourier transform) formats. One may also perceive that the numerator of the NCE estimate [(30)] has the form of a DFT relative to the Doppler-ratio variable q. This considerably reduces the required programming and the computational time in the realization of a NCE surface.

The variation in the τ-dimension, although not as expedient to reproduce, involves incremental translations of the one transform $V_m(k; J)$ relative to the other. When the equivalent bandwidth of the desired signal spectral power is greater than one-half the width of the spectral window, the scallop loss (due to discrete sampling in the τ-dimension) can exceed 1 dB and may approach 4 dB (when the equivalent bandwidth is equal to the width of the spectral window). Under these circumstances, the scallop loss can be reduced by computing a second series of $V_m(k; J)$ (for one of the signals), which is temporally interlaced with the original set. This is equivalent to choosing T_1 to be $1/2B_J$ for the one signal, and then sequentially interlacing the odd and even sets of resulting sectionalized Fourier transforms in computing the NCE estimate.

Although somewhat complicated, the indicated techniques (or modified versions thereof) for computing rather extensive ambiguity surfaces have been accomplished with relative ease on suitable array processors within the past decade [18]-[20], [31].

Validation of the NCE Estimate

The algorithm for estimating the NCE [given by (30)] can be applied in two ways. First, it can be used to study the ambiguity surface features for a broad class of temporal functions. And second, it can be used to detect (and estimate the parameters for) common signals which differ in time alignment and/or Doppler ratio.

In the first application, $V_{1,m}(k; J) = V_{2,m}(k; J)$ and the parameters q and m_τ are used to map the autocorrelation envelope over the $\tau\alpha$-plane. Letting the spectral window be centered on (and encompass) the spectral energy of the signal

[2] R. D. Trueblood of the Naval Ocean Systems Center (NOSC) employed this technique in connection with the magnitude-squared coherence (MSC) estimate in the early 1970's. The results of his (and subsequently other's) investigations indicated that the compensation was adequate for the signals and parameters used in the MSC estimate.

$u(t)$, it is seen that (30) closely approximates [from (18) and (20)]

$$\hat{\chi}_{k_0}(\tau, \alpha) = \frac{|\langle e^{i\pi mq'/M} V_{1,m-m_\tau}(k_0; J) V^*_{2,m}(k_0 + n_\alpha; J)\rangle|}{\sqrt{\langle |V_{1,m-m_\tau}(k; J)|^2\rangle \langle |V_{2,m}(k_0 + n_\alpha; J)|^2\rangle}}$$
$$= \frac{|\langle u_0(mT_1 - \tau')\mu_0^*\{(1 + \alpha')mT_1\} e^{-i2\pi m[\alpha_0 v_2(mT_1) - \alpha' v_2'(mT_1)]/B_J}\rangle|}{\sqrt{\langle |u_0(mT_1 - \tau')|^2\rangle \langle |u_0\{(1 + \alpha')mT_1\}|^2\rangle}} \tag{36a}$$

$$\hat{\chi}_{k_0}(\tau, \alpha) = \frac{|\langle u_0(mT_1 - \tau) u_0^*\{(1 - \alpha)mT_1\} e^{-i2\pi m\alpha v_2(mT_1)/B_J}\rangle|}{\sqrt{\langle |u_0(mT_1 - \tau)|^2\rangle \langle |u_0\{(1 + \alpha)mT_1|^2\rangle}} \tag{34a}$$

where

$$\tau = m_\tau/B_J \quad \text{and} \quad \alpha = -qB_J/2Mf_c. \tag{34b}$$

When both m_τ and q are zero, the NCE estimate equals unity. Further, along the τ axis ($\alpha = 0$), the estimate of the NCE is essentially precise. However, when α is nonzero, the estimate is degraded as a consequence of the nonlinear phase-distortion factor. (The degree that this factor influences the NCE estimate will be determined shortly.)

In the second application, consider that the common signal is $u(t)$ [see (1)] and that $s_1(t) = u(t + \tau_0)$ and $s_2(t) = u(t + \alpha_0 t)$. In this application, the parameters τ_0 and α_0 are unknown and will need to be estimated from the NCE function topology. (The NCE estimate is expected to peak at the point where τ and α compensate for the parameters τ_0 and α_0, respectively.) In practice, m_τ and q are systematically sequenced over a set of values which will encompass the anticipated range of τ_0 and α_0. Since the intent of the processing is to compensate for time and Doppler differences in the received signals, it will be advantageous to shift the spectral window periodically as discussed in relation to (17). (The shift in the spectral window function is to ensure that the two spectral windows span approximately the same portion of the signal spectrum in the common signal.)

An algorithm for determining the bin-shift parameter is developed as follows. With M [see (30b)] chosen so that M/J is an integer, let q' be a modulo integer defined as

$$q' = (q - jM/J) \text{ Mod } (2jM/J) - jM/J \tag{35a}$$

where j ($j \leqslant J$) is the desired number of Fourier transform bins to be translated with each modulo sequence. (When J is small, it may be expedient to make $j = 1$; however, when J is large, computation time can be saved by translating the spectral window in larger increments without seriously degrading the sensitivity of the correlation processor.) The shift parameter n_α is then

$$n_\alpha = (q - q')J/2M \tag{35b}$$

or, in terms of n_α, the value of q is

$$q = \frac{2M}{J} n_\alpha + q'. \tag{35c}$$

From (12), (18), and (20) then, it may be verified (with a little algebraic manipulation) that

where

$$\tau' = \tau - \tau_0 = m_\tau/B_J - \tau_0 \tag{36b}$$

$$\alpha' = \alpha_0 - \alpha = \alpha_0 - qB_J/2Mf_c \tag{36c}$$

$$v_2(mT_1) = v\{(1 + \alpha_0/2)mT_1\} \tag{36d}$$

and

$$v_2'(mT_1) = v\{(1 + \alpha'/2)mT_1\}. \tag{36e}$$

The above relation verifies that the NCE estimate is an accurate representation of the NCE, except for the nonlinear phase-distortion factor in the numerator. Of course, when $\alpha = 0$ ($q = 0$ and $\alpha' = \alpha_0$) the estimate is precise, provided the spectral energy of both signals falls within the spectral window. (This results from the fact that no Doppler compensation has been employed. The nonlinear phase-distortion is due solely to the convenient method chosen for Doppler compensation.) When $m_\tau/B_J - \tau_0$ is equal to $-\epsilon_1/B_J$ ($-1/2 \leqslant \epsilon_1 < 1/2$) and $\alpha_0 - qB_J/2Mf_c$ is equal to $\epsilon_2 B_J/2Mf_c$ ($-1/2 \leqslant \epsilon_2 < 1/2$), the estimate will maximize and equals

$$\hat{\chi}_{k_0}(\tau, \alpha) = |\langle R_m e^{i\pi\epsilon_1[v_1(mT_1)/B_J/2]} e^{i\pi(m/M)\epsilon_2}$$
$$\cdot e^{-i\pi m\alpha_0[v_2(mT_1)/B_J/2]}\rangle| \tag{37a}$$

where

$$R_m = |u_0(mT_1)|^2/\langle |u_0(mT_1)|^2\rangle = A^2(mT_1)/\langle A^2(mT_1)\rangle \tag{37b}$$

$$\tau = \tau_0 - \epsilon_1/B_J \qquad (-1/2 \leqslant \epsilon_1 < 1/2) \tag{37c}$$

$$\alpha = \alpha_0 - \epsilon_2 B_J/2Mf_c \qquad (-1/2 \leqslant \epsilon_2 < 1/2) \tag{37d}$$

$$v_1(mT_1) = v\{(m + \epsilon_1/2)T_1\} \tag{37e}$$

and

$$v_2(mT_1) = v\{(1 + \alpha_0/2)mT_1\}. \tag{37f}$$

Except for the three exponential degradation factors, the above estimate is equal to one (the desired value). The first two exponential factors degrade the estimate as a consequence of sampling the NCE function at discrete points along the τ and α axis of the ambiguity plane. This results in a two-dimensional scallop loss (in the estimate) over the $\tau\alpha$-plane. When ϵ_1 and ϵ_2 are zero, these factors reduce to one. The third exponential factor degrades the estimate as a consequence of the imperfect method of compensating for time scale-factor compression (or expansion) in the algorithm. The design considerations which may be employed to limit the degradation of the NCE estimate will now be addressed.

Expected Degradation of the NCE Estimate

The NCE estimate given by (37) is a function of the variables ϵ_1, ϵ_2, α_0, v, and A, and the design parameters M and B_J. The variables ϵ_1, ϵ_2, and v are zero-mean random processes, while A is either constant or is comprised of a mean value with a random component (over the analysis interval). For purpose of the analysis to follow, it will be reasonable to assume that the random processes are all ergodic and statistically independent.

A study of (36) and (37) reveals that the amplitude function $A(mT_1)$ can significantly influence the NCE estimate if this function is highly unstationary. For example, suppose that $A(mT_1)$ for a particular m is much greater than M times the value for the remainder of the set of m. In this event, the value of the NCE estimate given by (36) will approximately equal one regardless of the phase variation over m. This is a nontrivial problem and has occurred in practice in connection with transient signals of short duration (comparable to the sample period T_1). It can readily be perceived that the effect of relatively high-level transient bursts in the amplitude level is to shorten the effective (or useful) integration time of the NCE estimate. This in turn reduces (rather than increases) the degradation effects under consideration. Consequently, to obtain a useful measure of the degradation effects of the phase parameters under consideration, the amplitude parameter R_m will be considered as constant over the integration time. This procedure will maximize the phase misalignment degradation effects of the NCE estimate, which is of primary concern in this paper. Therefore letting $R_m = 1$, the expected degradation will be determined for each of the three factors in (37) separately.

Degradation due to sampling error ϵ_2: Consider first that ϵ_1 and α_0 are both zero. The value of the NCE estimate due to the error ϵ_2 becomes [23]

$$\begin{aligned}\hat{\chi}_{k_0}(\tau_0, -\epsilon_2 B_J/2Mf_c) &= \left|\frac{1}{M}\sum_{m=-M/2}^{M/2-1} e^{-i\pi(m/M)\epsilon_2}\right| \\ &= \frac{\sin(\epsilon_2\pi/2)}{M\sin(\epsilon_2\pi/2M)} \approx \frac{\sin(\pi\epsilon_2/2)}{\pi\epsilon_2/2} \leqslant \frac{4}{\pi}\sin(\pi/4) = 0.90.\end{aligned} \tag{38a}$$

Thus, the expected degradation due to imperfect α alignment will be less than about 0.91 dB. Further, since the probability density function for ϵ_2 will be constant over the range $-1/2 \leqslant \epsilon_2 < 1/2$, the expected degradation (averaging over ϵ_2) will be

$$2\int_0^{1/2} \frac{\sin(\pi\epsilon_2/2)}{\pi\epsilon_2/2}\, d\epsilon_2 = \frac{\mathrm{Si}(\pi/4)}{\pi/4} \approx 0.96\ (-0.33\ \mathrm{dB}). \tag{38b}$$

Thus, the increment sample size along the α dimension appears to be suitably chosen for practical applications.

Degradation due to sampling error ϵ_1: Consider next that ϵ_2 and α_0 are both zero. Assuming that $1 \ll M$, the NCE estimate may be closely approximated as

$$\begin{aligned}\hat{\chi}_{k_0}(\tau, 0) &= \left|\frac{1}{M}\sum_{m=-M/2}^{M/2-1} e^{i2\pi\epsilon_1 v_1(mT_1)/B_J}\right| \\ &\simeq \left|\frac{1}{T}\int_{-T/2}^{T/2} e^{i2\pi\epsilon_1 v(t)/B_J}\, dt\right| \\ &= \left|\frac{1}{T}\int_{-T/2}^{T/2} \cos\left[2\pi\epsilon_1 v(t)/B_J\right] dt \right. \\ &\qquad \left. + i\int_{-T/2}^{T/2} \sin\left[2\pi\epsilon_1 v(t)/B_J\right] dt\right|.\end{aligned} \tag{39a}$$

Since $v(t)$ is a zero-mean function over the analysis interval, the imaginary term of the NCE estimate will be near zero and the real term can be expected to dominate over the permissible range of ϵ_1 and $v(t)$. Although the expected value of the imaginary term will be zero, it does not follow that the expected value of the NCE estimate will be determined by the real term alone. However, it does follow that a lower bound on the expected value of the estimate can be determined by using only the real term. And as long as the real term does not become small compared to one, it will closely approximate the true expected value of the estimate. Thus

$$\hat{\chi}_{k_0}(\tau, 0) \geqslant \left|\frac{1}{T}\int_{-T/2}^{T/2} \cos\left[2\pi\epsilon_1 v(t)/B_J\right] dt\right|. \tag{39b}$$

And letting $p_v(v)$ be the probability density function of v and assuming that $p_v(-v) = p_v(v)$, the lower bound on the expected value of the NCE estimate (when ϵ_1 is given) is

$$\begin{aligned}E\{\hat{\chi}_{k_0}(\tau, 0)\} &\geqslant 2\int_0^\infty p_v(v)\cos(2\pi\epsilon_1 v/B_J)\, dv \\ &= 2\int_0^\infty p_\theta(\theta)\cos\theta\, d\theta\end{aligned} \tag{39c}$$

where $\theta = 2\pi\epsilon_1 v/B_J$ and $p_\theta(\theta) = (B_J/2\pi\epsilon_1)p_v(B_J\theta/2\pi\epsilon_1)$.

The above relation has been solved for three probability density functions, and the results are tabulated in Table III. The first probability density is the case where v is uniformly distributed over a bandwidth B_v. The second is a Gaussian function whose standard deviation is limited to a maximum of $B_J/4$. (The bandwidth B_v is the information bandwidth of the signal (see [30, pp. 229-236].) The probability density for the third case is realized when v is a sinusoidal fluctuation whose peak-to-peak frequency excursion is uniformly distributed over the bandwidth B_v [33].[3]

From the table one can observe that the expected degradation will depend on B_v and the distribution of v over B_J, as well as the sampling error ϵ_1. For $|\epsilon_1| = 1/2$ and B_v at its maximum permitted value, the lower bound of the expected

[3]The three probability density functions considered here, as well as a number of other distributions, may be found in [33]. This earlier work demonstrates that the coherence degradation will depend essentially on the standard deviation of the θ variable (and be relatively independent of the probability density function) when σ_θ is less than one.

TABLE III
PROBABILITY DENSITY AND EXPECTED NCE ESTIMATES RELATING TO THE SAMPLING ERROR ϵ_1

	PROB. DENSITY $p_v(v)$	σ_v/B_v	$E\{\hat{\chi}_{k_0}(\tau,0)\}$
1	$1/B_v$ $(\lvert v\rvert \leqslant B_v/2)$	$1/2\sqrt{3}$ $B_v \leqslant B_J$	$\dfrac{\sin(\pi\epsilon_1 B_v/B_J)}{\pi\epsilon_1 B_v/B_J}$
2	$\dfrac{1}{B_v}e^{-\pi v^2/B_v^2}$ $(\lvert v\rvert \leqslant B_J/2)$	$1/\sqrt{2\pi}$ $B_v \leqslant \sqrt{\pi/8}\,B_J$	$e^{-\pi(\epsilon_1 B_v/B_J)^2}$
3	$\dfrac{2}{\pi B_v}\ln\left[\dfrac{B_v+\sqrt{B_v^2-4v^2}}{2\lvert v\rvert}\right]$ $(\lvert v\rvert \leqslant B_v/2)$	$1/2\sqrt{6}$ $B_v \leqslant B_J$	$\dfrac{B_J}{\pi\epsilon_1 B_v}\int_0^{\pi\epsilon_1 B_v/B_J} J_0(x)\,dx$ $\approx e^{-\frac{\pi^2}{12}(\epsilon_1 B_v/B_J)^2}$

degradation in each case will be: 0.637 (-3.92 dB) in case 1, 0.735 (-2.68 dB) in case 2, and 0.814 (-1.79 dB) in case 3. Since the error ϵ_1 will be uniformly distributed over the range $-1/2 \leqslant \epsilon_1 < 1/2$, the expected degradation due to this cause in each case (averaging over ϵ_1) will be limited to

$$\frac{\mathrm{Si}(\pi B_v/2B_J)}{\pi B_v/2B_J} \leqslant \frac{\mathrm{Si}(\pi/2)}{\pi/2} = 0.873\ (-1.18\ \mathrm{dB}),$$

$$\frac{B_J}{B_v}\,\mathrm{erf}\left(\frac{\sqrt{\pi}}{2}\,\frac{B_v}{B_J}\right) \leqslant 2\sqrt{\frac{2}{\pi}}\,\mathrm{erf}\left(\frac{\pi}{4\sqrt{2}}\right) = 0.905\ (-0.86\ \mathrm{dB}),$$

and

$$2\sqrt{\frac{3}{\pi}}\,\frac{B_J}{B_v}\,\mathrm{erf}\left(\frac{\pi}{4\sqrt{3}}\,\frac{B_v}{B_J}\right) \leqslant 2\sqrt{\frac{3}{\pi}}\,\mathrm{erf}\left(\frac{\pi}{4\sqrt{3}}\right) = 0.93\ (-0.59\ \mathrm{dB})$$

where the error function erf (z) is defined as [24, pp. 295-300]

$$\mathrm{erf}(z) = \frac{2}{\sqrt{\pi}}\int_0^z e^{-x^2}\,dx.$$

This amount of degradation appears tolerable for practical application. However, the expected degradation can be further reduced by sampling the one channel at twice the Nyquist interval and interlacing the sample sets in (30) as described earlier. In this event, Table III will still be applicable with the understanding that ϵ_1 is limited to $\pm 1/4$.

Degradation due to imperfect Doppler compensation: Finally, consider that ϵ_1 and ϵ_2 are both zero. Assuming $1 \ll M$, the NCE estimate in this situation may be written

$$\begin{aligned}\hat{\chi}_{k_0}(\tau_0,\alpha_0) &= \left|\frac{1}{M}\sum_{m=-M/2}^{M/2-1} e^{-i2\pi\alpha_0 mT_1 v_2(mT_1)}\right| \\ &\simeq \frac{1}{T}\left|\int_{-T/2}^{T/2}\cos\left[2\pi\alpha_0 tv(t)\right]dt\right. \\ &\quad \left. + i\int_{-T/2}^{T/2}\sin\left[2\pi\alpha_0 tv(t)\right]dt\right| \\ &\geqslant \left|\frac{1}{T}\int_{-T/2}^{T/2}\cos\left[2\pi\alpha_0 tv(t)\right]dt\right| \qquad (40)\end{aligned}$$

where $T = (M-1)T_1 = (M-1)/B_J$. Again, letting $p_v(v)$ be the probability density of v and assuming that $p_v(-v) = p_v(v)$, the lower bound on the expected value of the NCE estimate becomes

$$\begin{aligned}E\{\hat{\chi}_{k_0}(\tau_0,\alpha_0)\} &\geqslant \frac{4}{T}\int_0^\infty p_v(v)\left|\int_0^{T/2}\cos(2\pi\alpha_0 tv)\,dt\right|dv \\ &= 2\int_0^\infty p_v(v)\left|\frac{\sin(\pi\alpha_0 Tv)}{\pi\alpha_0 Tv}\right|dv \\ &\geqslant 2\int_0^\infty p_v(v)\,\frac{\sin(\pi\alpha_0 Tv)}{\pi\alpha_0 Tv}\,dv \\ &= \int_0^1\left[2\int_0^\infty p_v(v)\cos(\pi\alpha_0 Tvx)\,dv\right]dx. \qquad (41)\end{aligned}$$

One may recognize that the inner integral in (41) is identical in form to (39c). Consequently, the results given in Table III will be applicable to this case provided $\alpha_0 B_v Tx/2$ is substituted for $\epsilon_1 B_v/B_J$. The lower bound on the expected values of the NCE estimate (for the three given probability densities) may therefore be computed as

$$\frac{\mathrm{Si}(\pi\alpha_0 B_v T/2)}{\pi\alpha_0 B_v T/2} \qquad (42a)$$

$$\frac{\mathrm{erf}(\sqrt{\pi}\alpha_0 B_v T/2)}{\alpha_0 B_v T} \qquad (42b)$$

and

$$\frac{\mathrm{erf}(\pi\alpha_0 B_v T/4\sqrt{3})}{\sqrt{\pi}\alpha_0 B_v T/2\sqrt{3}}. \qquad (42c)$$

Since the above expectations are derived from ensemble averages for the random variable $v(t)$, it will be informative to determine the error in the NCE estimate for specific examples of $v(t)$ for comparison purposes. Two examples are chosen which produce rather severe degradation on the estimate. In the first example let

$$v(t) = \pm B_v t/T \qquad (-T/2 \leqslant t \leqslant T/2) \qquad (43a)$$

and in the second example let

$$v(t) = \begin{cases}\pm B_v/2 & (\text{for } 0 < t \leqslant T/2) \\ \mp B_v/2 & (\text{for } -T/2 \leqslant t \leqslant 0)\end{cases}. \qquad (43b)$$

In the first example, the frequency varies linearly from $\mp B_v/2$ to $\pm B_v/2$ over the integration period T. This is representative of what can occur in practice. However, it is a severe example in that $v(t)$ is perfectly correlated with the integration variable t (which will maximize the degradation due to the linear frequency slide). In the second example, the frequency $v(t)$ remains fixed at $\pm B_v/2$ for one-half the integration time and then flips to the negative value for the remainder of the integration period. This is an extreme case which will be approached infrequently in practice. However, it will provide a suitable upper bound on the expected NCE degradation.

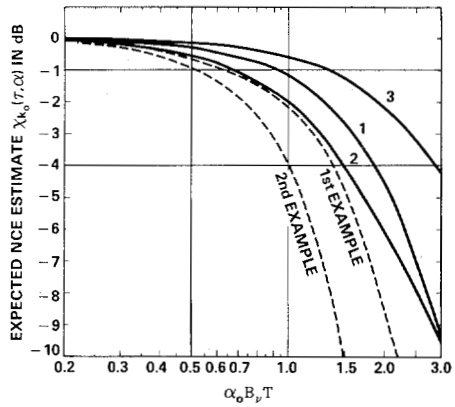

Fig. 6. Coherence degradation due to imperfect Doppler compensation as a function of $\alpha_0 B_v T$. (Curves labeled 1, 2, and 3 result from assuming the corresponding probability densities given in Table III.)

Employing the two specific examples in (40) and carrying out the integration gives

$$\hat{\chi}_{k_0}(\tau_0, \alpha_0) = \frac{C(\sqrt{|\alpha_0| B_v T})}{\sqrt{|\alpha_0| B_v T}} \tag{44a}$$

for the first example, where $C(\cdots)$ is the Fresnel cosine integral of the indicated argument [24, pp. 300–304], and

$$\hat{\chi}_{k_0}(\tau_0, \alpha_0) = \left| \frac{\sin(\pi \alpha_0 B_v T/2)}{\pi \alpha_0 B_v T/2} \right| \tag{44b}$$

for the second example. Graphs of these functions along with those given in (42) are shown in Fig. 6.

The curves (Fig. 6) illustrate that the value of $\alpha_0 B_v T$ should be limited to about one if excessive degradation due to imperfect Doppler compensation is to be avoided. Since all of the curves are above −1 dB for $\alpha_0 B_v T$ equal to (or less) than 0.5, this value would represent a conservative choice for $\alpha_0 B_v T$.[4] Therefore, a reasonable upper bound on the integration parameter M is [from (31)]

$$M \leq \frac{1}{|\alpha_0|} \frac{B_J}{B_v} + 1. \tag{45a}$$

And since the Doppler ratio α_0 is $\Delta v_0/c$, where Δv_0 is the difference in source speed along the propagation paths to the two signal sensors and c is the signal propagation speed in the transmission medium [30]

$$M \leq \frac{c}{|\Delta v_0|} \frac{B_J}{B_v} + 1 \geq \frac{c}{|\Delta v_0|} + 1. \tag{45b}$$

In the case of underwater acoustic applications, c is approximately 2880 knots. Assuming a source-speed differential of 10 knots, a suitable bound for M is less than or equal to $288\, B_J/B_v$.

Summary and Conclusions

Although the Fourier transform of a temporal function is normally used to decompose the function into its complex spectral components, the sectionalized Fourier transform (SFT) may be employed in a manner which preserves the temporal properties of the original signal. It has been demonstrated that when a contiguous sequence of J SFT spectral bins is appropriately summed (J typically being a small number), the resulting transform of a band-limited signal is equivalent to basebanding, filtering, and sampling the signal in the time domain. The value of J may be chosen to control the passband and leakage characteristics of the filter (see Figs. 1–4).

With the advent of the FFT algorithm and modern array processors, use of the SFT to baseband, filter, and sample signals considerably simplifies the programming of multidimensional correlation processors in practical applications. Further, using the ambiguity kernel as an approximation of signal time compression (or expansion), the FFT algorithm is applicable to correlation mapping along the Doppler-ratio axis of the ambiguity plane. The resulting error has been shown to be negligible when the product of the signal bandwidth and the correlator integration time is less than the inverse of the maximum Doppler ratio being employed. Using the techniques described in this paper (and modification thereof), two-dimensional correlation mapping of low-frequency acoustical signals over long integration intervals has been implemented for the NCE estimate (or the MSC estimate) well in excess of real time.

It may be concluded that the sectionalized Fourier transform has many applications as an alternate (and convenient) method of time-domain processing using modern array digital computers. Its application is limited only by the sample rate which can be processed in the digital computer employed.

Appendix
Expected Value of the Distortion Function

From (3) and (5), the distortion function may be written in the form

$$D_m(g_m, J) = \frac{1}{T_2} \int_{-T_2/2}^{T_2/2} A_m F(t) e^{i2\pi(\delta_c + T_2 \bar{v}_m) t/T_2}\, dt \tag{A1a}$$

where

$$A_m = A_j(mT_1 + t)/A_j(mT_1) \tag{A1b}$$

$$\bar{v}_m = \frac{1}{t} \int_0^t v_k(mT_1 + x)\, dx \tag{A1c}$$

and

$$F(t) = \sin(\pi J t/T_2)/\sin(\pi t/T_2) \tag{A1d}$$

and with the additional provisions that $A_j(mT_1) > 0$ and $\pm 1/2$ is added to δ_c when J is even [as described in the text following (5)].

The function $F(t)$ is deterministic, while the functions A_m and $\bar{v}_m$ are comprised of sample functions (A_j and v_k) drawn from ensembles (or sets) with common statistical characteristics. To emphasize this fact, (A1a) is rewritten as

$$D_{mjk} = \frac{1}{T_2} \int_{-T_2/2}^{T_2/2} A_{mj} F(t) e^{i2\pi(\delta_c + T_2 \bar{v}_{mk}) t/T_2}\, dt \tag{A2}$$

where the subscripts j and k have been attached to the sample function A_m and $\bar{v}_m$ to imply that a sample member from

[4] W. H. Marsh [19] has recommended that $\alpha_0 B_v T$ be limited to less than 0.25 in connection with the MSC estimate. However this appears to be ultraconservative in light of the results displayed in Fig. 6.

each ensemble $\{A_j\}$ and $\{v_k\}$ is chosen in the computation of the distortion function.

The expected value of the above distortion function is obtained by computing the integral averaged over the double ensemble of sample functions. In computing the ensemble averages it will be assumed that the two sample sets are independent, and the sample functions A_j and v_k from each ensemble are both ergodic and stationary over the integration interval T_2. (The condition of stationary does not apply to the functions A_{mj} and $\bar{v}_{mk}$ which are constructed from A_j and v_k.) Restrictions on the properties of A_j and v_k to qualify as a member of each ensemble will be determined as we proceed with the analysis. (Basically, the members of each ensemble must be such that their interrelated power spectral density is confined to fall essentially within the spectral window of J/T_2 Hz.) Under the stipulated conditions, the expected value of the distortion function becomes

$$E\{D_m\} = \langle D_{mjk}\rangle \quad \text{(averaged over } j, k\text{)}$$

$$= \frac{1}{T_2}\int_{-T_2/2}^{T_2/2} \langle A_{mj}\rangle F(t) e^{i2\pi\delta_c t/T_2}\langle e^{i2\pi\bar{v}_{mk}t}\rangle\, dt. \tag{A3a}$$

Letting $p_1(A_m, t)$ and $p_2(\bar{v}_m, t)$ denote the time-variable probability densities of A_m and $\bar{v}_m$, respectively, the respective ensemble averages can be written

$$\langle A_{mj}\rangle = \int_0^\infty A_m p_1(A_m, t)\, dA_m \tag{A3b}$$

and

$$\langle e^{i2\pi\bar{v}_{mk}t}\rangle = \int_{-\infty}^{\infty} p_2(\bar{v}_m, t) e^{i2\pi\bar{v}_m t}\, dv_m. \tag{A3c}$$

At this point it is important to realize that the restrictions on the member functions of the two independent ensembles are interrelated. The functions $\{A_{mj}\}$ are amplitude modulations of the carrier functions $\exp\{i2\pi[\delta_c/T_2 + \bar{v}_{mk}]t\}$. A member of this carrier set is $\exp\{i2\pi[\delta_c/T_2 + v_M]t\}$, where v_M is the extreme limit of a slowly varying fluctuation frequency. Therefore, since any dynamic variation in the sample function A_{mj} will produce equal sidebands of power on either side of the carrier frequency $\delta_c/T_2 + v_M$, [35] the carrier frequency must be restricted to lie sufficiently well within the spectral window to accommodate the amplitude modulation sidebands. On this basis it is evident that when J is one and $\delta_c = 1/2$, A_m must be essentially constant over T_2 if the distortion function is not to become excessive. On the other hand, when J is large, the parameter δ_c will not play a significant role in restricting the members of the ensembles. Consequently, for $1 \ll J$, the spectral window need be only sufficiently broad to accommodate both the maximum deviation in the frequency fluctuation $v(t)$ and the spectral sidebands introduced as a consequence of the amplitude modulation (if significant distortion of the resulting transformed signal is to be avoided).

Since the two ensembles of sample functions are assumed independent, it will be convenient and appropriate to treat the amplitude and frequency fluctuation problems separately.

Expected Distortion Due to Frequency Fluctuations

Consider first that the functions $\{A_j(mT_1 + t)\}$ are essentially constant over time increments of T_2 seconds such that the ensemble $\{A_{mj}\}$ is unity. Considering then the broad class of ensemble functions $\bar{v}_{mk}$, it is reasonable to assume that for every member function there exists a member function which has its negative time characteristics. This is equivalent to assuming that $p_2(\bar{v}_m, -t) = p_2(\bar{v}_m, t)$. With these considerations, (A1a) reduces to

$$E\{D_m\} = \frac{2}{T_2}\int_0^{T_2/2}\int_{-\infty}^{\infty} p_2(\bar{v}_m, t)\frac{\sin(\pi Jt/T_2)}{\sin(\pi t/T_2)} \cdot \cos[2\pi(\delta_c + T_2\bar{v}_m)t/T_2]\, d\bar{v}_m\, dt. \tag{A4}$$

It is well to note that the maximum time we need be concerned with is $T_2/2$. However, the magnitude of the Dirichlet kernel decays rapidly for t greater than $T_2/2J = T_1/2$. Consequently, the significance of $p_2(\bar{v}_m, t)$ becomes increasingly less beyond $t = T_1/2$.

Since $\bar{v}_{mk}$ is the running-time average of $v_k(mT_1 + t)$, its probability density function will depend on the dynamic characteristics (or power spectrum) of $v(t)$ as well as on the smoothing time t. It should also be apparent that the peak magnitude of $\bar{v}_{mk}$ cannot exceed the peak magnitude of $v_k(mT_1 + t)$ (that is, $|\bar{v}_{mk}| \leqslant |v_k(mT_1 + t)|$). When t is sufficiently small so that $v_k(mT_1 + t)$ is approximately equal to $v_k(mT_1) + \dot{v}_k(mT_1)t$ over all members of the ensemble, the probability density of $\bar{v}_m$ will approximate the probability density of v. On the other hand, when t is large, the probability density of $\bar{v}_m$ will be compressed relative to the probability density of v. This is evident since the average of a rapidly varying zero-mean function approaches zero over relatively long time intervals.

To exemplify the above consideration, let

$$v_k(mT_1 + t) = v_M \sin(2\pi\rho t + \phi_m)$$

where v_M is the frequency deviation ($v_M \leqslant B_J/2 = J/2T_2$) and ρ is the modulating frequency. Then

$$\bar{v}_{mk}(t) = \frac{1}{t}\int_0^t v_k(mT_1 + x)\, dx$$

$$= v_M \frac{\sin \pi\rho t}{\pi\rho t}\sin(\pi\rho t + \phi_m)$$

$$= \frac{\sin \pi\rho t}{\pi\rho t} v_k(mT_1 + t - t/2).$$

Thus, $\bar{v}_{mk}$ is a delayed (by the amount $t/2$) and compressed version of the function $v_k(mT_1 + t)$. The ratio v_M/ρ is known as the frequency modulation index of the process, and the resulting signal spectral energy can be expressed in terms of Bessel functions. To prevent significant spectral energy of the signal from exceeding the passband of the spectral window, this ratio should be no greater than $\pi/2$ [36]. This places an upper bound on the modulating frequency ρ of $2v_M/\pi \leqslant B_J/\pi$.

Using the upper bound for ρ, the function $\bar{v}_{mk}$ becomes

$$\bar{v}_{mk}(t) = \frac{\sin(2v_M t)}{2v_M t} v_k(mT_1 + t - t/2)$$

and for $|t|$ less than or equal to $T_1/2$, the compression factor is

$$\frac{\sin(2v_M t)}{2v_M t} \leqslant \frac{\sin v_M T_1}{v_M T_1} \leqslant 2\sin(1/2) \approx 0.96.$$

Thus, in the extreme case (for ρ maximum allowable), the probability density for $\bar{v}_m$ will be approximately the same as the probability density for v, within the primary lobe of the Dirichlet kernel. The maximum rate of change of $v_k(mT_1 + t)$ is $2\pi\rho v_M \leqslant 4v_M^2 \leqslant B_J^2 = J^2/T_2^2$. This rate limits the change in $v_k(mT_1 + t)$ over the period of T_1 s to less than the spectral window width of B_J hertz (or equivalently, $\dot{v}T_1^2 \leqslant 1$). Little error will therefore result in assuming that the probability density of $\bar{v}_m$ is the same as the probability density of v over T_2.

As a consequence of the above analysis, (A4) will closely approximate [using (6a)]

$$E\{D_m\} \simeq \int_{-\infty}^{\infty} p_v(v) \int_0^1 \frac{\sin(\pi Jt/2)}{\sin(\pi t/2)} \cdot \cos[\pi(\delta_c + T_2 v)t]\, dt dv$$

$$= \int_{-\infty}^{\infty} p_v(v) W_J(\delta_c + T_2 v)\, dv \qquad \text{(A5)}$$

where $p_v(v)$ is the probability density function for v and $W_J(\cdots)$ is the spectral window function for the indicated argument.

The expected value of the distortion function is therefore the weighted value of the magnitude of the spectral window function (see Figs. 1 and 2). The weighting function is the probability density function for the fluctuating frequency v. When $J \gg 1$, $W_J(x)$ is approximately equal to one over the spectral window passband. Therefore if $p_v(v)$ is zero for $|v| > B_J/2$, the expected value of the distortion function is essentially unity.

Expected Distortion Due to Amplitude Fluctuations

To study the expected distortion due to amplitude modulation we shall consider that $v(mT_1 + t)$ is constant over $-T_2/2 \leqslant t \leqslant T_2/2$, and let $x_m = \delta_c + T_2 v(mT_1)$. The ensemble average will be taken only over j holding k fixed, so that (A3a) becomes

$$E_k\{D_m\} = \langle D_{mjk} \rangle \quad \text{(averaged over } j\text{)}$$

$$= \frac{1}{T_2} \int_{-T_2/2}^{T_2/2} \langle A_{mj} \rangle \frac{\sin(\pi Jt/T_2)}{\sin(\pi t/T_2)} e^{i2\pi x_m t/T_2}\, dt. \qquad \text{(A6)}$$

To proceed, it will prove convenient to perform the ensemble averaging in steps. First, it may be assumed that for every member function A_{mj} there exists a complement member function with negative time characteristics. Thus, the average of the member and its complement is an even function of time. As a consequence, the expected value of the distortion will be real and we need carry the averaging process only over even functions of time. The symbology A_{mj} will henceforth be used to represent an even function of time, with the understanding that the first step of ensemble averaging has been effected.

Next, let $A_j(mT_1 + t)$ be written as $A_{0j}[1 + a_j(t)]$, where A_{0j} is the mean value over the time interval T_2 and a_j is a zero-mean function greater than -1 over this interval. Then A_{mj} takes the form $[1 + a_j(t)]/[1 + a_j(0)]$. Over the time interval T_2, $a_j(t)$ may be expanded into the Fourier series

$$a_j(t) = \sum_{p=1}^{P} b_{jp} \cos(2\pi pt/T_2)$$

where

$$a_j(0) = \sum_{p=1}^{P} b_{jp} > -1.$$

Since no significant spectral energy will be permitted to fall outside of the spectral window, the ensemble of functions a_j to be considered will be limited to those whose upper limit P is restricted by the relation

$$P \leqslant J/2 - |x_M|$$

where $|x_M|$ is the maximum excursion of the frequency fluctuation x_m. This informs us that when J is either less than 2 or $|x_M|$ is $J/2$, no significant amplitude modulation can be permitted without serious distortion of the resulting transformed signal. If one-half of the spectral window is reserved for frequency modulation, P will be limited to values less than $J/4$.

With the above considerations then, (A6) reduces to

$$E_k\{D_m\} = \left\langle \int_0^1 \frac{1 + \sum_{p=1}^{P} b_{jp} \cos(\pi pt)}{1 + a_j(0)} \frac{\sin(\pi Jt/2)}{\sin(\pi t/2)} \cdot \cos(\pi x_m t)\, dt \right\rangle$$

$$= \left\langle \left[\sum_{p=-P}^{P} b_{j|p|} W_J(x_m + p) \right] \Big/ \sum_{p=-P}^{P} b_{j|p|} \right\rangle \qquad \text{(A7)}$$

where $b_{j0} = 2$ and $W_J(\cdots)$ is the spectral window function [defined in (6)] for the indicated argument.

The above relation shows that the expected signal distortion due to amplitude fluctuations will be dependent on the flatness of the spectral window over the passband. Thus, when J is sufficiently large so that the spectral window can be assumed to be unity over the passband, (A7) reduces to one.

ACKNOWLEDGMENT

The author is indebted to his colleague W. L. Anderson for criticism and suggestions regarding the applications of the ensemble averaging techniques employed in the analysis. Mr. Anderson has also written the computer code for programming the NCE estimate algorithms discussed in this paper, and has demonstrated these algorithms in undersea acoustic applications. Credit is due to E. L. Kunz for the programming and computation of the illustrations shown in the paper. Our

thanks also to Dr. T. Kooij who managed and supervised this work for the Tactical Technology Office of the Defense Advanced Research Projects Agency.

REFERENCES

[1] J. W. Cooley and J. W. Tukey, "An algorithm for the machine calculation of complex Fourier series," *Math. Comput.*, vol. 19, pp. 297-301, 1965.

[2] W. T. Cochran, J. W. Cooley, *et al.*, "What is the fast Fourier transform?" *IEEE Trans. Audio Electroacoust.*, vol. AU-15, pp. 45-55, 1967.

[3] J. R. Fisher, "Fortran program for fast Fourier transform," NRL Rep. 7041, Apr. 1970.

[4] G. C. Carter, "Estimation of the magnitude-squared coherence function," NUSC Tech. Rep. 4343, May 1972.

[5] G. C. Carter and A. H. Nuttall, "Statistics of the estimate of coherence," *Proc. IEEE*, vol. 60, no. 4, pp. 465-466, 1972.

[6] —, "Evaluation of the statistics of the estimate of magnitude-squared coherence," NUSC Tech. Memo. TC-193-71, Sept. 1971.

[7] G. C. Carter, C. H. Knapp, and A. H. Nuttall, "Estimation of the magnitude-squared coherence function via overlapped fast Fourier transform processing," *IEEE Trans. Audio Electroacoust.*, vol. AU-21, pp. 337-344, 1973.

[8] —, "Statistics of the estimate of the magnitude coherence function," *IEEE Trans. Audio Electroacoust.*, vol. AU-21, no. 4, pp. 388-389, 1973.

[9] G. C. Carter, A. H. Nuttall, and P. G. Cable, "The smoothed coherence transform," *Proc. IEEE*, vol. 61, pp. 1497-1498, 1973.

[10] G. C. Carter and C. H. Knapp, "Coherence and its estimation via the partitioned modified chirp-z transform," *IEEE Trans. Acoust., Speech, Signal Processing*, vol. ASSP-23, pp. 257-264, 1975.

[11] A. H. Nuttall and G. C. Carter, "Approximations for statistics of coherence estimators," NUSC Tech. Rep. 5291, Mar. 1976.

[12] J. J. Gosselin, "Comparative study of two-sensor magnitude-squared coherence and single-sensor square-law receiver operating characteristics," *Proc. IEEE ICASSP-77*, vol. 6, pp. 311-314, 1977.

[13] E. H. Scannell, Jr., and G. C. Carter, "Confidence bounds for magnitude-squared coherence estimates," *Proc. IEEE ICASSP-78*, pp. 670-673, 1978.

[14] R. Lugannani, "Distribution of the sample magnitude-squared coherence; the overlap case," NOSC Rep. 78-005, Oct. 1978.

[15] N. R. Goodman, "On the joint estimation of the spectra, cospectrum, and quadrature spectrum of a two-dimensional stationary Gaussian process," Sci. Paper 10, Eng. Stat. Lab., New York Univ., 1957.

[16] R. Merk, "Statistics of average magnitude-squared coherence," NOSC Rep. 77-014, Apr. 1978.

[17] A. S. Greenstein, "Intersensor coherent processing-theoretical results," General Electric Rep. DA 140-525, 1976.

[18] R. D. Trueblood and D. L. Alspach, "Multiple coherence as a test statistic," NOSC Rep. TR-265, July 1978.

[19] W. H. Marsh, "Correction of inaccuracies in estimation of the narrowband ambiguity surface," NOSC Rep. TR 257, June 1978.

[20] J. Malony, "Coherent cross-correlation with different bandwidths in each channel," ENSCO, Inc., unpublished, report available from the author.

[21] H. Dym and H. P. McKean, *Fourier Series and Integrals*. New York: Academic, 1972, pp. 31-35.

[22] C. Lanczos, *Discourse on Fourier Series*. New York: Haffner, 1966, pp. 29-30.

[23] H. B. Dwight, *Tables of Integrals and Other Mathematical Data*, 4th ed. New York: Macmillan, 1961, p. 92, eqs. 420.2-420.4.

[24] M. Abramowitz and I. A. Stegun, Eds., *Handbook of Mathematical Functions*, Applied Mathematics Series 55. Washington, DC: NBS, 1964, pp. 300-329.

[25] M. Schwartz, W. R. Bennett, and S. Stein, *Communication Systems and Techniques*. New York: McGraw-Hill, 1966, pp. 82-85.

[26] J. S. Bendat, *Principles and Applications of Random Noise Theory*. New York: Wiley, 1958, pp. 55-60.

[27] D. Linden, "A discussion of sampling theorems," *Proc. IRE*, vol. 47, pp. 1219-1226, 1959.

[28] F. J. Harris, "On the use of windows for harmonic analysis with the discrete Fourier transform," *Proc. IEEE*, vol. 66, no. 1, pp. 51-83, 1978.

[29] D. Gingras, "Time series windows for improving discrete spectra estimation," NOSC Rep. NUC TN-715, Apr. 1972.

[30] A. A. Gerlach, *Theory and Applications of Statistical Wave-Period Processing*, vol. 1. New York: Gordon and Breach, 1970; pp. 97-100.

[31] —, "Impact of the ocean acoustic transfer function on the coherence of undersea propagations," *IEEE Trans. Acoust., Speech, Signal Processing*, vol. ASSP-28, pp. 145-158, 1980.

[32] P. M. Woodward, *Probability and Information Theory with Applications to Radar*. London: McGraw-Hill, 1953, pp. 115-123.

[33] A. A. Gerlach, "Motion induced coherence degradation in passive systems," *IEEE Trans. Acoust., Speech, Signal Processing*, vol. ASSP-26, pp. 1-15, 1978.

[34] —, "Role of the sectionalized Fourier transform in high-speed coherence processing," NRL Rep. 8438, Oct. 16, 1980.

[35] M. Schwartz, W. R. Bennett, and S. Stein, *Communications Systems and Techniques*. New York: McGraw-Hill, 1966, pp. 173-176.

[36] —, *Communications Systems and Techniques*. New York: McGraw-Hill, 1966, pp. 225-228.

[37] —, *Communications Systems and Techniques*. New York: McGraw-Hill, 1966, pp. 120-121.

Albert A. Gerlach (S'42-A'46-SM'50) received the B.S. degree from the Ohio State University in 1942, the M.S. in electrical engineering in 1949, the M.S. in math in 1951, and the Ph.D. in 1958 from the Illinois Institute of Technology.

He served as a Radar Officer during World War II, and since 1946 he has been engaged in a variety of government-sponsored research and development activities spanning the gamut of electromagnetics, nuclear, aerospace, medical electronics, and underwater acoustics. He has been associated with several commercial firms including the Illinois Institute of Technology Research Institute and the Cook Electric Company. At the latter he served as an Associate Director and Director of Research for the Cook Technology Center Division. Since 1971 he has been with the Acoustics Division of the Naval Research Laboratory conducting signal processing research in underwater acoustics.

Dr. Gerlach has been active in a number of scientific and professional societies over the past thirty years, serving on a number of technical committees including Chairman of the Chicago Section of IEEE and founder and Chairman of the Chicago Chapter PGCT. He has published papers in several professional journals covering various areas of circuit theory, signal processing and underwater acoustics. He is the author of a three volume book, *Theory and Applications of Statistical Wave-Period Processing* (New York: Gordon and Breach, 1970).